OCEANOGRAPHY

Marine emissions of methanethiol increase aerosol cooling in the Southern Ocean

Charel Wohl[1,2]†, Julián Villamayor[3]†, Martí Galí[1]†, Anoop S. Mahajan[4], Rafael P. Fernández[5], Carlos A. Cuevas[3], Adriana Bossolasco[3,6], Qinyi Li[7], Anthony J. Kettle[8], Tara Williams[9], Roland Sarda-Esteve[10,11], Valérie Gros[10], Rafel Simó[1]*, Alfonso Saiz-Lopez[3]*

Ocean-emitted dimethyl sulfide (DMS) is a major source of climate-cooling aerosols. However, most of the marine biogenic sulfur cycling is not routed to DMS but to methanethiol (MeSH), another volatile whose reactivity has hitherto hampered measurements. Therefore, the global emissions and climate impact of MeSH remain unexplored. We compiled a database of seawater MeSH concentrations, identified their statistical predictors, and produced monthly fields of global marine MeSH emissions adding to DMS emissions. Implemented into a global chemistry-climate model, MeSH emissions increase the sulfate aerosol burden by 30 to 70% over the Southern Ocean and enhance the aerosol cooling effect while depleting atmospheric oxidants and increasing DMS lifetime and transport. Accounting for MeSH emissions reduces the radiative bias of current climate models in this climatically relevant region.

INTRODUCTION

In the sulfate-rich ocean, around 50% of the sulfur assimilated by marine primary producers is routed to the methylated sulfonium compound dimethylsulfoniopropionate (DMSP) (*1*–*3*). With a global production rate of ~2 Pg S year^{-1} (*4*), this labile metabolite channels a large share of reduced sulfur cycling in upper-ocean microbial food webs (*5*) and its biological degradation releases volatile sulfur (*2*, *6*). Subsequent sea-to-air emission and atmospheric oxidation of this biogenic sulfur fuel the formation and growth of sulfate and methanesulfonate aerosols (*7*, *8*), which cool the Earth by scattering sunlight [direct radiative effect (DRE)] and increasing cloud albedo [indirect radiative effect (IRE)] (*7*, *9*). The climatic importance of marine sulfur emissions to the atmosphere is maximized in remote marine regions (*10*–*12*) far from the dominant effects of continental sulfur emissions of largely anthropogenic origin (*13*). Despite being among the most studied climate forcers, quantification of the radiative effects of sulfur aerosols remains a challenge for global climate models, especially in the Southern Ocean where notable radiative differences between climate model simulations and satellite observations suggest that the effects of natural aerosols are being underestimated (*10*).

Hitherto, dimethyl sulfide (DMS) has received all the attention as the main form in which the oceans emit aerosol-forming volatile sulfur (*2*, *7*). This has fostered decades of research from which global maps of seawater DMS concentrations became available (*14*) to be implemented in climate models (*12*). Yet, only around 15% of the DMSP consumed by marine microbes is routed to DMS according to in situ rate measurements (*2*, *15*, *16*). The remainder is mostly routed through the demethylation pathway, which ultimately results in reduced sulfur assimilation but produces methanethiol (MeSH) through an intermediate demethiolation step (*2*, *6*). The demethylation/demethiolation pathway is ubiquitous in upper-ocean metagenomes and metatranscriptomes (*1*, *17*, *18*), implying a large potential for MeSH production that is also supported by sensitive radiotracer measurements (*15*) and by the observation of MeSH release by cultured marine bacterial strains upon DMSP addition (*19*–*22*). Despite the biochemically proven relevance of marine MeSH production, analytical difficulties arising from high MeSH reactivity to metals and surfaces (*6*) have hindered extensive surveys of MeSH in seawater, let alone global-scale mapping. The few existing measurements of concentrations in seawater (*23*, *24*), marine air (*25*–*27*), tank experiments (*28*), and sea-to-air fluxes (*26*) consistently indicate that MeSH represents a substantial proportion of the ocean's volatile methylated sulfur (VMS) (i.e., DMS and MeSH) pool and emission. However, factors controlling this proportion and the MeSH distribution are unclear, which hindered previous global emission estimates.

Atmospheric chemistry pathways for VMS indicate that MeSH oxidation is faster and has a higher effective sulfur dioxide (SO_2) yield than DMS oxidation (*26*), hence greater potential for aerosol formation. However, climate models used in international climate assessments, such as those included in the Sixth Assessment Report of the Intergovernmental Panel on Climate Change (*29*), have so far omitted marine MeSH emissions, arguably as a consequence of the poor knowledge of seawater MeSH concentrations and subsequent emissions to the atmosphere. Here, we assess MeSH and DMS coemission patterns on the global scale through the compilation and analysis of new and available measurements and use a state-of-the-art global climate model to quantify the impact of added sulfur from MeSH on atmospheric chemistry and aerosol radiative forcing. Our results show that MeSH emission causes a large and nonlinear increase in the atmospheric burden of VMS. The additional formation of SO_2 from MeSH ultimately translates into a shortwave radiative cooling due to increased sulfate aerosol (SO_4^{2-}) that is largest over the Southern Ocean.

[1]Department of Marine Biology and Oceanography, Institut de Ciències del Mar, CSIC, Barcelona, Catalonia, Spain. [2]Centre of Ocean and Atmospheric Sciences, University of East Anglia, Norwich, UK. [3]Department of Atmospheric Chemistry and Climate, Institute of Physical Chemistry Blas Cabrera, CSIC, Madrid, Spain. [4]Centre for Climate Change Research, Indian Institute of Tropical Meteorology, Ministry of Earth Sciences, Pune, India. [5]Institute for Interdisciplinary Science (ICB), National Research Council (CONICET), FCEN-UNCuyo, Mendoza, Argentina. [6]Physics Institute of Northwest Argentina (INFINOA), National Research Council (CONICET), Tucumán, Argentina. [7]Environment Research Institute, Shandong University, Qingdao, China. [8]Météo France, Lannion, France. [9]Old Dominion University, Norfolk, VA, USA. [10]Laboratoire des Sciences du Climat et de l'Environnement (LSCE), CNRS-CEA-UVSQ, IPSL, Gif sur Yvette, France. [11]Climate and Atmosphere Research Center (CARE-C), the Cyprus Institute, Nicosia, 2121, Cyprus.
*Corresponding author. Email: rsimo@icm.csic.es (R.S.); a.saiz@csic.es (A.S.-L.)
†These authors contributed equally to this work.

RESULTS

Marine MeSH emission

We compiled surface seawater measurements of concurrently measured MeSH and DMS from all available cruises (see Materials and Methods), namely, AMT7 (temperate and tropical Atlantic, September to October 1998) (*23*), TRANSSIZ (Nordic Seas, May to June 2015) (*24*), and OC1607A and OC1708A (Northeast Pacific, July 2016 and August 2017). To these data, we added unpublished measurements from the POLAR-CHANGE cruise (Southern Ocean, February to March 2023) and year-round measurements from the Blanes Bay observatory (Mediterranean Sea, 2022). The resulting dataset (Fig. 1A) covers a wide range of latitude (67.8°S to 80.9°N), sea surface temperature (SST) (−0.7° to 31.7°C), and biological productivity as proxied by chlorophyll a (Chl a) concentration (0.04 to 18.04 μg dm^{-3}). The mean (median) surface ocean MeSH concentration is 0.78 (0.57) nmol dm^{-3}, with lower and upper quartiles of 0.35 and 0.91 nmol dm^{-3}. For the same measurement points, the mean DMS concentration is 2.32 nmol dm^{-3}, which is close to the global mean (*14*).

Our analysis reveals that MeSH linearly, but moderately, correlates with concurrently measured DMS ($R^2 = 0.49$, P value < 0.001, $n = 584$). The statistical fit between MeSH and DMS improves by defining two regimes based on in situ SST and bathymetry thresholds (Fig. 1B). We coin them the high and low MeSH:DMS regimes. Measurements taken on continental shelves (bathymetry < 250 m) fall into the low MeSH:DMS regime, independent of SST. The remaining, open-ocean measurements fall into the low MeSH:DMS regime for an SST above 12°C, and into the high MeSH:DMS regime for an SST below 8°C. Although the 8°C cutoff provides an optimal regime separation in our dataset (Fig. 1B), the regime-specific linear fits between MeSH and DMS are statistically indistinguishable for cutoff temperatures between 8° and 12°C but degrade outside this range (see Materials and Methods). Thus, on a global scale, the SST and shelf sea versus open ocean seem to control the ratio between MeSH and DMS concentrations in seawater.

The fitted model implies a bimodal distribution of the MeSH:DMS concentration ratio, with interquartile ranges of 0.39 to 0.65 and 0.10

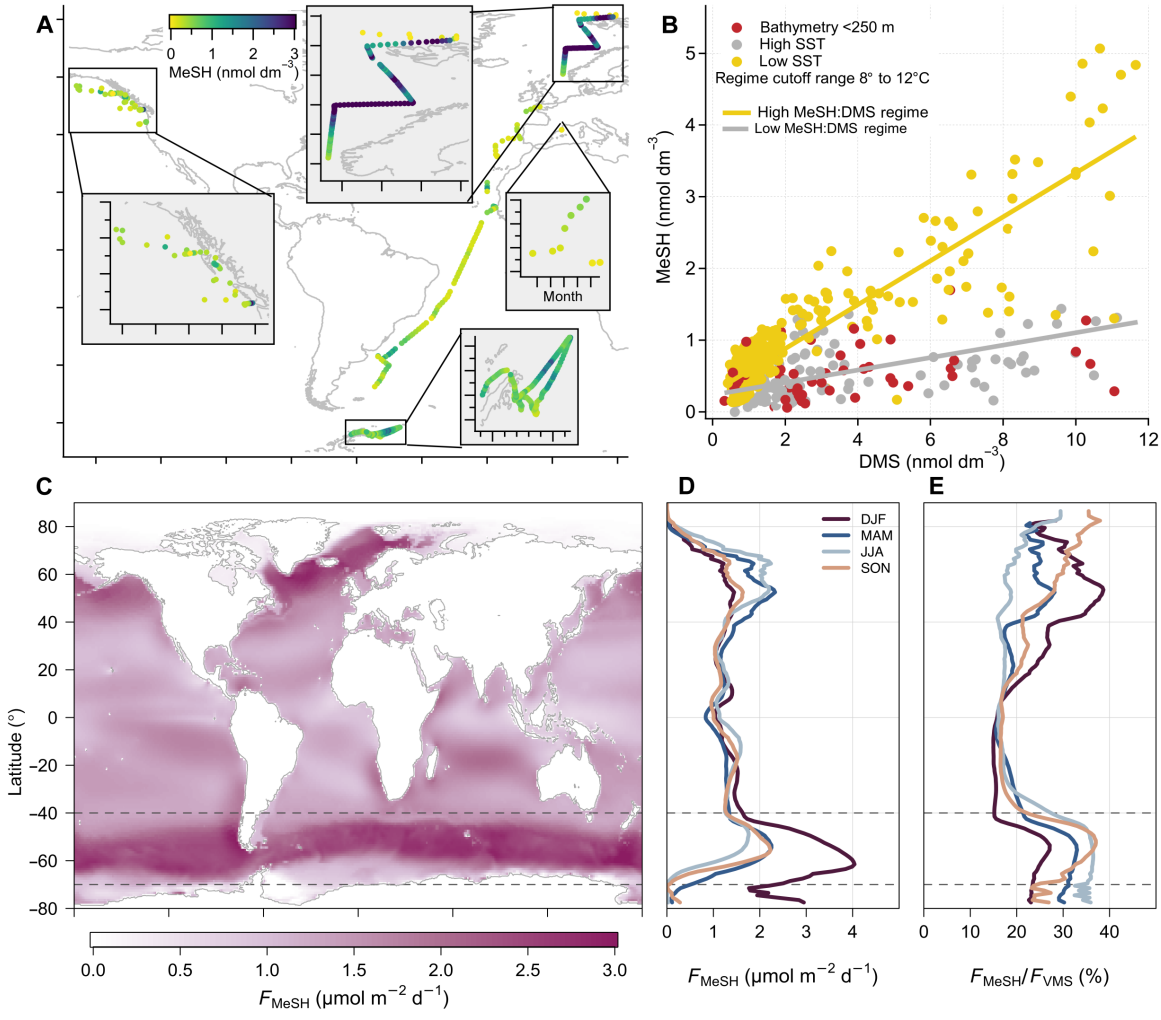

Fig. 1. Large scale patterns of MeSH concentrations and emission fluxes. (**A**) Geographical distribution of the in situ measurements. The points are colored by the seawater MeSH concentration (cut off at 3 nmol dm^{-3}). (**B**) Scatter plot illustrating data point classifications (using a cutoff temperature of 8°C) and the linear fits for the high and low MeSH:DMS regimes. (**C**) Annual mean sea-to-air flux of MeSH (F_{MeSH}). (**D**) Zonal mean MeSH sea-to-air flux. d, day. (**E**) Zonal mean contribution of MeSH to VMS sea-air fluxes (F_{MeSH}/F_{VMS}). Zonal means in (D) and (E) are colored by seasons. The horizontal dashed lines in (C), (D), and (E) bound the Southern Ocean area.

to 0.32 in the high and low regimes, respectively. The significant positive intercepts of the regressions between MeSH and DMS result in high MeSH:DMS ratios at very low DMS and MeSH concentrations. Variability in the MeSH:DMS ratio likely reflects the effects of various environmental drivers on the dynamic balance between the sources and sinks of each compound. Laboratory cultures of widespread marine bacterial strains showed MeSH:DMS production ratios of around 1:3 (*19*, *22*) and 1:1 (*21*) upon DMSP addition. In natural samples, Kiene and Linn (*15*) found a much higher MeSH:DMS production ratio of ~7:1 using trace additions of radiolabeled DMSP. Unlike DMS, most of the produced MeSH was rapidly (<3 hours) assimilated by microorganisms, implying a large difference between gross and net MeSH yields. The same study suggested lower MeSH assimilation (hence higher MeSH yields) at lower temperatures and offshore, consistent with observed MeSH:DMS patterns (Fig. 1B). Besides biological consumption (*6*, *15*, *30*), fast scavenging by dissolved organic matter and metals (*2*, *6*, *15*) and photochemical loss (*31*, *32*) would keep aqueous MeSH concentrations below DMS ones. As a result, dissolved MeSH appears to turn over much faster (<1 to 7 hours; $n = 11$) (*6*) than DMS (1 to 6 days; $n = 196$) (*16*). Given the current state of knowledge, explanations for the variability in the MeSH:DMS concentration ratio remain speculative. Nonetheless, our analysis indicates that variability in this ratio must be accounted for to quantify the atmospheric effects of MeSH and DMS emission.

The two-regime empirical model allowed the construction of monthly global ocean fields of MeSH seawater concentrations and emissions, drawing from climatological DMS concentrations (*14*), observational SST fields, and bathymetry. Combining the constructed monthly fields of sea surface MeSH concentration with concurrent monthly fields of SST and 10-m wind speed (the three variables on which the air-sea flux depends the most; see Supplementary Methods), we calculate a global annual MeSH emission of 5.7 ± 0.6 Tg S year^{-1}, with a corresponding global annual DMS emission of 23.5 Tg S year^{-1}. The confidence interval reported for MeSH emission corresponds to the $\pm 2\sigma$ range of a statistical ensemble of sea surface MeSH fields obtained through bootstrapping while keeping DMS and geophysical fields fixed (see Supplementary Methods). The DMS emission reported here is based on a state-of-the-art gas transfer parameterization, lowering by 13% a previous benchmark estimate (*14*).

Oceanic MeSH emissions peak at the high latitudes during each hemispheric summer (Fig. 1D), similar to DMS (*14*). Yet, the proportion between MeSH and DMS emission fluxes is far from constant across regions and seasons (Fig. 1E). The contribution of MeSH to the total VMS emission spans from around 15 to 20% in the tropics to around 25 to 37% in the subpolar oceans. Globally and annually, MeSH accounts for 19% of the revised global ocean biogenic sulfur emissions with largest contributions to the polar oceans' sulfur flux. Covering 21% of the global ocean area, the Southern Ocean 40°S to 70°S latitude band accounts for an equivalent proportion (21%) of global marine VMS emissions but around 27% of global MeSH emissions, owing to higher MeSH:DMS ratios in cold ocean waters.

Atmospheric methylated sulfur burden

Monthly sea-to-air MeSH fluxes were included in the Community Atmosphere Model with interactive chemistry (CAM-Chem, version 4) (*33*, *34*), along with an updated sulfur chemistry scheme (see Materials and Methods). Our simulations were conducted using a specified dynamics setup (*34*) nudged to the Modern-Era Retrospective analysis for Research and Applications version 2 (MERRA2) reanalysis representing the 5-year period of 2018 to 2022. Sensitivity tests confirmed the robustness of our simulation setup against uncertainties in the updated sulfur chemical scheme and the newly developed MeSH emission field presented in this work (see Materials and Methods). This allows us to confidently quantify the MeSH contribution to the atmospheric VMS, SO_2, and SO_4^{2-} burdens by analyzing the difference between a simulation including the MeSH flux ("MeSH") and a baseline run with the same model configuration but omitting the MeSH flux ("noMeSH").

The results reveal that adding MeSH emissions to the model increases the annual global mean VMS atmospheric burden by 34% (Fig. 2). This enhancement is particularly pronounced in the Southern Ocean between 40°S and 70°S, where the annual mean VMS burden increases by a remarkable 51% when MeSH emission is considered. Thus, including MeSH emissions increases the atmospheric VMS burden by more than the MeSH emissions themselves add alone. This is explained by a concomitant increase in the DMS burden by 11% globally and 17% over the Southern Ocean, despite DMS sea-to-air fluxes remaining unchanged. MeSH emission, therefore, not only adds new sulfur but also increases the DMS burden, the latter accounting for one-third of the overall VMS increase (Fig. 2D). This amplification also exhibits seasonal variation, peaking in the summer, when the DMS enhancement accounts for nearly half of the total VMS increase over the Southern Ocean (fig. S1).

The amplification of the DMS burden is caused by a MeSH-mediated depletion of oxidants (OH, BrO, NO_3, and Cl) that react with both species (Fig. 2C and fig. S2). Because of MeSH's shorter oxidative lifetime (*23*, *26*), MeSH efficiently competes with DMS for oxidants. This competition alters the concentration of oxidants and, consequently, the vertical distribution of DMS concentration and the altitude of DMS oxidation (fig. S3). The presence of MeSH effectively decreases DMS loss near its oceanic emission sources, extending its local chemical lifetime by 1.2 days in the Southern Ocean lower troposphere (averaged below 850 hPa). Globally averaged, the atmospheric lifetimes of DMS and MeSH are 2.1 and 1.5 days, respectively. The extended lifetime of DMS leads to a wider spatial VMS distribution, both vertically and meridionally, away from the main source regions (Fig. 2C).

Sulfate aerosol DRE

Accounting for MeSH emissions leads to an enhancement of SO_2 production, doubling its budget near the surface of the ocean around 65°S (Fig. 3A). This, in turn, enhances SO_4^{2-} aerosol formation over the Southern Ocean. The strongest increase in SO_4^{2-} production occurs near the area with the highest MeSH emission around 65°S. In the regional lower troposphere, this increase exceeds 70%. The enhancement in SO_4^{2-} extends vertically and meridionally, with up to 10% additional SO_4^{2-} reaching the mid-troposphere (~500 hPa), and is noticeable in the lower troposphere from the tropics to the South Pole (Fig. 3A). The impact of MeSH emission on sulfate aerosol, hence, extends across the Southern Hemisphere.

Our simulations show that increased SO_4^{2-} associated with MeSH emissions exerts a large increase in aerosol cooling centered over the Southern Ocean, with an average annual increase in the sulfate DRE (see Supplementary Methods) of 28% between 40°S and 70°S and a peak increase of 50% around 65°S (Fig. 3A). The DRE exhibits strong seasonality, reaching a maximum of -0.075 W m^{-2}

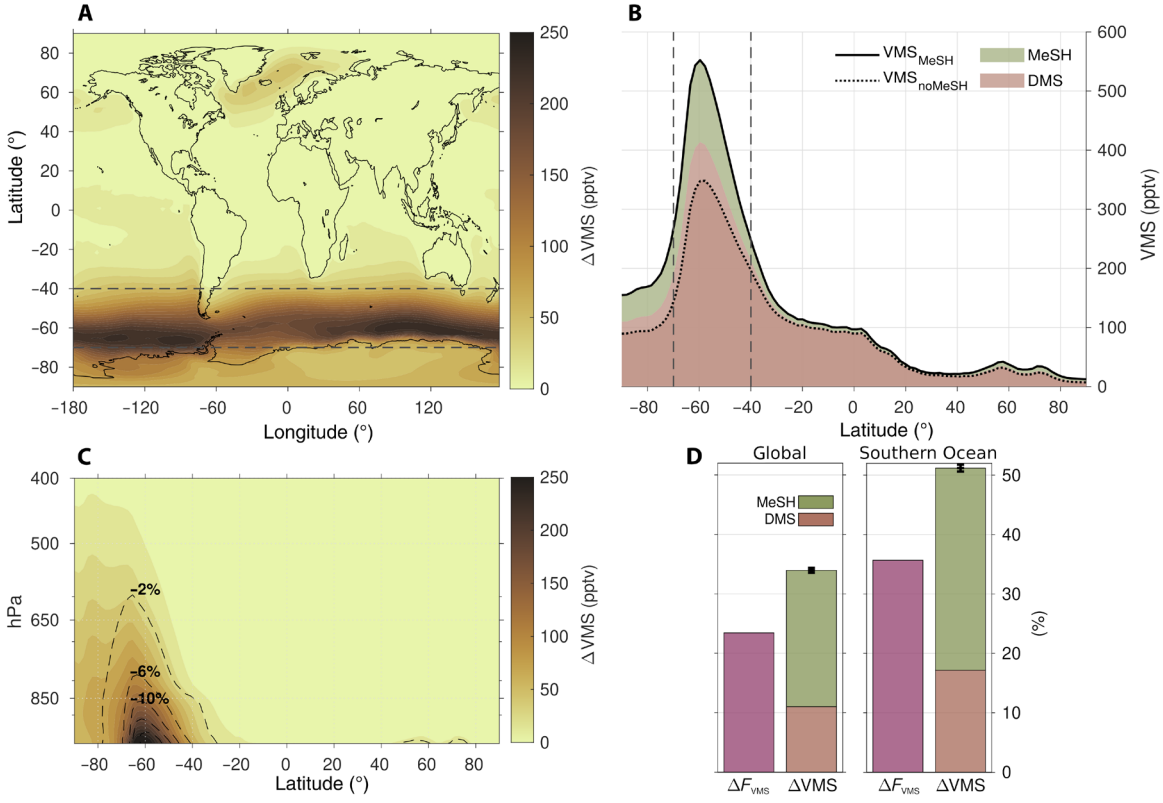

Fig. 2. Increase in the tropospheric annual mean burden of VMS accounted for by MeSH emissions. (**A**) ΔVMS averaged in the lower troposphere (below 850 hPa) in parts per trillion by volume (pptv). (**B**) Meridional distribution of the zonal mean lower troposphere VMS in the "noMeSH" (dashed line) and "MeSH" (solid line) simulations, the latter decomposed into the MeSH (green shade) and DMS (brown shade) shares. (**C**) Vertical distribution of zonal mean ΔVMS (shading) and relative change of OH (dashed contours). (**D**) Bar charts of the relative increase (%) of the VMS emission flux (purple) and the total atmospheric VMS burden (green for MeSH and brown for DMS) averaged globally (left) and over the Southern Ocean (right). Error bars show the 95% confidence interval of ΔVMS. Dashed lines in (A) and (B) bound the Southern Ocean.

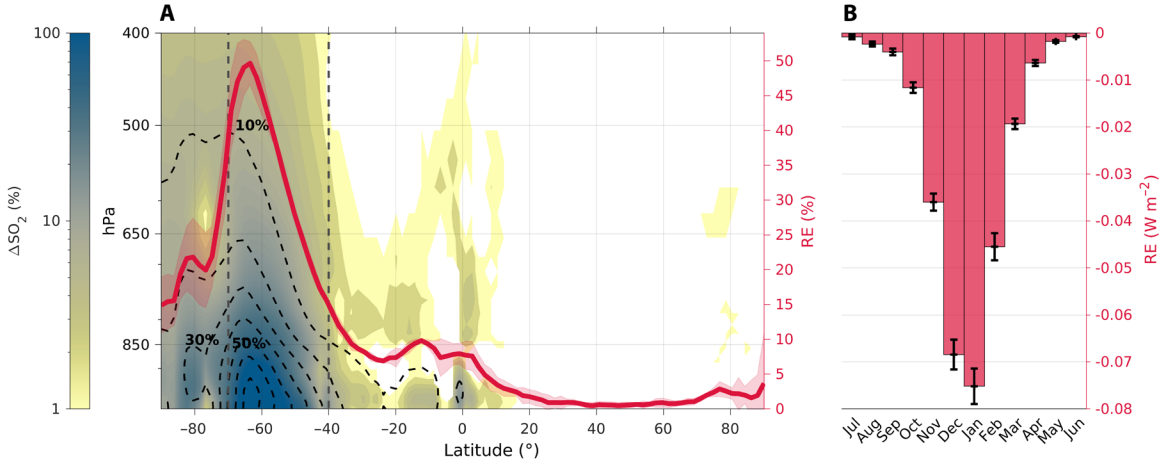

Fig. 3. Increase in the annual mean tropospheric burdens of SO_2 and SO_4^{2-} and the radiative effect accounted for by MeSH emissions. (**A**) Vertical distribution of the zonal mean relative change of sulfur dioxide (ΔSO_2; color shading) and sulfate aerosol (ΔSO_4^{2-}; black dashed contours) and the relative amplification of the SO_4^{2-} DRE (red line in %; right axis). The vertical dashed lines bound the Southern Ocean. (**B**) Seasonal variation of the SO_4^{2-} DRE averaged in the Southern Ocean (W m^{-2}) ± the 95% confidence interval (error bars).

in January (mid-summer) (Fig. 3B). This coincides with the highest MeSH and DMS emissions and the peak in solar irradiance that favor the largest increase in SO_2 and SO_4^{2-} formation in the summer (fig. S4).

The large anthropogenic contribution to the SO_4^{2-} burden outside of the pristine Southern Ocean dwarfs the global mean MeSH-mediated DRE, which increases by 4% (−0.016 W m^{-2}). To put this global effect in context, the absolute magnitude of MeSH-mediated DRE is about one-third of the warming that occurred over 1900 to 2015 resulting from mitigated anthropogenic SO_2 emissions (rounded to +0.05 W m^{-2}) (*35*).

Influence of MeSH on climate

From the aforementioned estimate of the present-day DRE of MeSH, the IRE of MeSH-derived sulfate aerosols through aerosol-cloud interactions over the Southern Ocean in the summer, yet largely uncertain, can be estimated to be −0.3 to −1.5 W m^{-2} in January, based on the 4- to 20-fold proportionality between the IRE and DRE of sulfate aerosols over the Southern Ocean (*36*, *37*). This is particularly relevant because current global climate models such as those of the Coupled Model Intercomparison Project phase 6 (CMIP6) present an as yet unresolved radiative bias of +4 to +15 W m^{-2} in the Southern Ocean in the summer (*10*), which has implications for regional and global climate simulations (*38*–*40*). The radiative bias consists of an excess of modeled shortwave solar radiation reaching the surface and is mainly attributed to the incorrect representation of cloud properties in climate models, including aerosol effects on cloud micro- and macrophysics (*39*). The peak of the overpredicted solar radiation occurs around 60°S to 65°S (*40*), coinciding with the peak of sulfate aerosols from MeSH emission. Therefore, our revised ocean sulfur emissions, with inclusion of MeSH, should contribute to reduce the modeled excess solar radiation in a region of major relevance for global climate.

DISCUSSION

The robust statistical predictors obtained in the construction of the global MeSH climatology reveal that the polar oceans constitute emission hotspots during the summer. Including the novel MeSH sea-to-air fluxes in an atmospheric chemistry-climate model results in a net radiative effect that has far-reaching implications (Fig. 4), especially over the pristine Southern Ocean, ranging from increases in the atmospheric burdens of VMS and SO_4^{2-} aerosols to a decrease in OH, which is the major atmospheric oxidant (fig. S2), along with enhanced transport of DMS and its oxidation products toward the equator, poleward, and further aloft. Besides contributing to aerosol radiative effects, MeSH causes changes in the oxidative capacity that indirectly affect other atmospheric species that contribute to the radiative balance, such as methane, halogens, and secondary aerosol-forming organics (*41*–*43*). Our results highlight MeSH as a previously overlooked agent that needs to be included in global climate models for accurate assessment of the atmospheric oxidative capacity and the radiative balance in the reconstruction of preindustrial scenarios as well as in projections of global warming as anthropogenic sulfur emissions continue to decline (*13*).

Almost four decades ago, the CLAW (for Charlson, Lovelock, Andreae & Warren) hypothesis (*7*) postulated that the marine biota act as a climate regulator through the emission of volatile sulfur into the atmosphere, its subsequent oxidation to form aerosols, and the large impacts of aerosols on dimming downwelling solar radiation. If the magnitude of volatile sulfur production by plankton, in turn, responded positively to solar radiation or seawater temperature, then a negative (regulatory) feedback would be in action between marine life and climate. The search for evidence for or against this hypothesis has focused on DMS as the only chemical form for marine sulfur emissions (*11*, *44*–*52*). Here, we show that the MeSH distribution, its biological and chemical cycling in the surface ocean, its interaction with sunlight and temperature, and its atmospheric chemistry must be experimentally quantified and numerically modeled in parallel to those of DMS when investigating the potential feedback between ocean-emitted biogenic sulfur and climate.

MATERIALS AND METHODS

BLANES 2022 and POLAR-CHANGE 2023 measurements

Mediterranean surface seawater sampling at the Blanes Bay Microbial Observatory was carried out monthly during 2022, except January, March, and April. Seawater was hand collected in glass sampling bottles around 11:00 a.m. and taken to the lab for analysis as described below. The POLAR-CHANGE cruise was conducted in February and March 2023 on board the BIO RV Hesperides A33 in waters of the Antarctic Peninsula and the Weddell Sea. A Vocus PTR-ToF (TOFWERK AG, Thun, Switzerland, Vocus Scout) coupled to a segmented flow coil equilibrator (SFCE) (*53*) was used to measure DMS and MeSH in seawater from the underway seawater inlet. Details on the operation of the Vocus will be largely reserved for a future manuscript describing the POLAR-CHANGE Southern Ocean measurements. A brief overview is provided here. To monitor instrument performance and drift, the Vocus was calibrated at least daily using a multicompound gas standard (nominal mole fraction 500 nmol mol^{-1} [= parts per billion by volume (ppbv)]; containing DMS, Apel-Riemer Environmental Inc., Miami, FL, United States) serially diluted in zero air (Vocus Clean Air System). The hourly zero air was used as a blank for the seawater equilibrator headspace measurement. With the Vocus, we found no indication that the SFCE permeates or emits DMS or MeSH. During the POLAR-CHANGE cruise, we observed extremely high MeSH concentrations at the beginning of the cruise. After cleaning the equilibrator daily with 10% HCl, concentrations dropped down to within previously observed ranges. We decided to exclude all MeSH measurements before regular cleaning commenced as these data points are likely affected by biofouling.

During deployments, measured equilibrator headspace ions per second of MeSH were converted to nmol mol^{-1} using the internal calibration curve of the instrument (= relationship between k_{PTR} and sensitivity and accounting for transmission efficiency). We assume a k_{PTR}(MeSH) of 1.8×10^{-9} cm^3 s^{-1}. Dissolved MeSH and DMS concentrations were calculated using published solubility values (*54*). We additionally calibrated the setup for MeSH by serial dilution of sodium methanethiolate in seawater in the laboratory (fig. S5).

The agreement between measured and expected calibration slopes or headspace mixing ratios confirms this approach of calculating dissolved MeSH concentrations. The limit of detection due to measurement noise is 0.0006 nmol dm^{-3} for DMS and 0.0019 nmol dm^{-3} for MeSH. We estimate that the total error of our measurements is less than 5% for DMS and 15% for MeSH.

MeSH database

Underway measurements from AMT7 were extracted from the graphs in the published manuscript using an image extraction

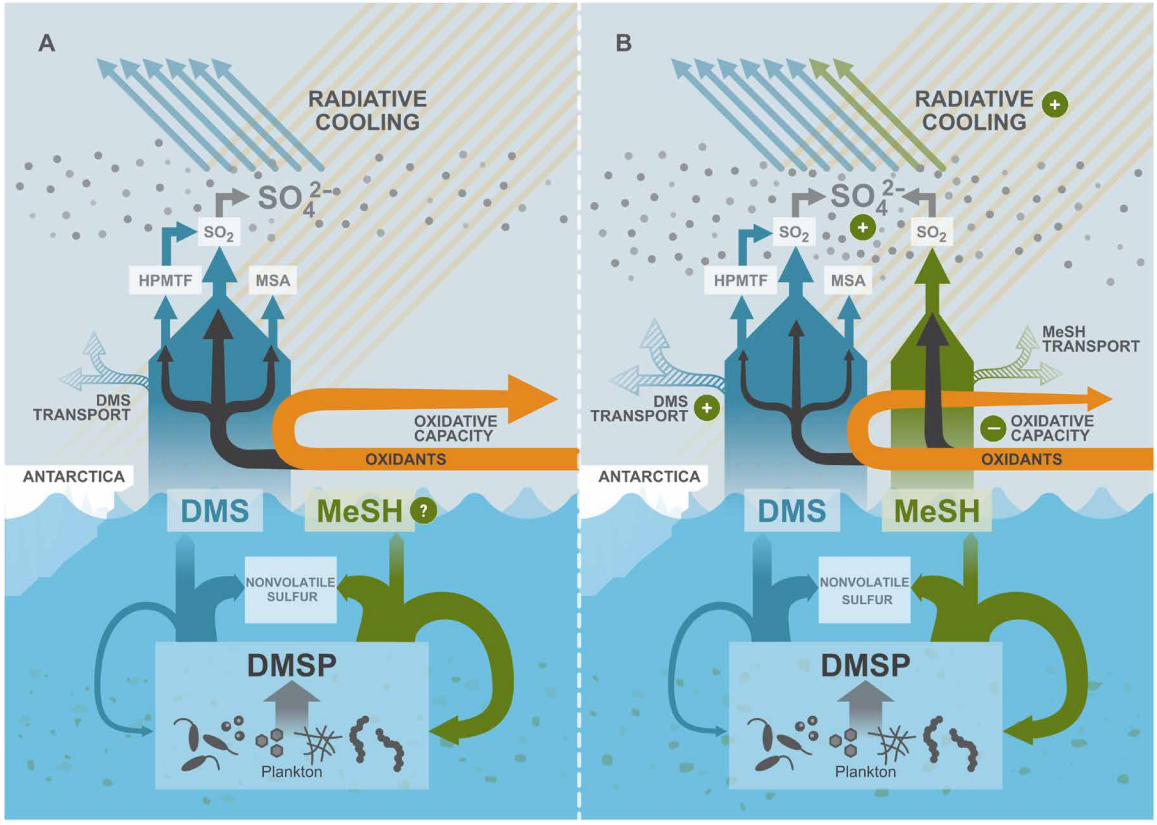

Fig. 4. Conceptual representation of the revised ocean-atmosphere sulfur cycle and the MeSH emission effects over the Southern Ocean. (**A** and **B**) In chemistry-climate models, DMS was hitherto considered the sole volatile sulfur compound emitted to the atmosphere (dark blue) from planktonic DMSP degradation. From observations, MeSH was known to be a DMSP degradation product with a substantial sea-to-air flux but not considered by climate models due to lacking global emission estimates. In the atmosphere, DMS reacts with oxidants (orange), initiating chemical chain reactions (black arrows) that ultimately form sulfur dioxide (SO_2) as the primary product, alongside secondary products like methanesulfonic acid (MSA) and intermediates like HPMTF (*12*, *51*). SO_2 further oxidizes to form sulfate aerosol (SO_4^{2-}) (gray dots), which exerts direct radiative cooling by reflecting and scattering downwelling solar radiation. (B) Including MeSH in chemistry-climate models has a substantial impact on the atmosphere. MeSH reacts faster than DMS with atmospheric oxidants (OH, BrO, NO_3, and Cl), effectively reducing the atmospheric oxidative capacity, extending DMS chemical lifetime near its emission source and facilitating its transport across latitudes and altitudes (blue dashed arrow). In addition, MeSH oxidation contributes to more SO_2 production (*26*). These combined effects lead to a broader distribution and increased production of SO_4^{2-}, ultimately enhancing the Southern Ocean's overall radiative cooling effect.

technique (https://apps.automeris.io/wpd/). To ensure concurrency of the measurements and deal with the error in the time stamp related to the use of an image extraction technique, data from AMT7 were binned in 6-hourly bins. Positional data for AMT7 are available online at https://bodc.ac.uk/resources/inventories/cruise_inventory/report/5625/. The data from cruises OC1607A and OC1708A are available online at https://hdl.handle.net/1912/27278. The data from the TRANSSIZ cruise are available online at https://doi.pangaea.de/10.1594/PANGAEA.953917. We binned data from the TRANSIZ and POLAR-CHANGE cruises into hourly bins to avoid over-representation of these high-resolution datasets. Bathymetry data were obtained by matching measurement coordinates with the General Bathymetric Chart of the Oceans (https://gebco.net/data_and_products/gridded_bathymetry_data/; GEBCO_2023 sub ice topo, last accessed March 2024).

Empirical model development

We decided to exclude eight surface CTD measurements from TRANSSIZ as there is a large discrepancy between underway and surface CTD MeSH concentrations reported from this cruise. We also excluded four measurement points from OC1607A with a Chl a concentration of more than 10 μg dm^{-3} as they could be affected by bloom-specific artifacts. Measurements with DMS > 12 nmol dm^{-3} were excluded from all cruises from the model development as they disproportionately affected our regression model and could also be affected by bloom-specific artifacts. The following number of MeSH concentration measurements is contributed to the database by each measurement campaign (in parentheses, measurements from each cruise containing SST and bathymetry data, with DMS < 12 nmol dm^{-3}): POLAR-CHANGE 356 (355), BLANES 2022 9 (9), TRANSSIZ 146 (73), AMT7 101 (85), and OC1607A 40 and OC1708A 28 (both 62).

The empirical model for MeSH prediction has thus been constructed using exclusively observational (in situ) datasets in the following ranges: MeSH, 0.07 to 5.0 nmol dm^{-3}; DMS, 0.33 to 11.7 nmol dm^{-3}; Chl a, 0.04 to 19.7 μg dm^{-3}; SST, −0.7° to 31.7°C; and latitude, −67.8° to 80.3°. This DMS range covers 99% of the climatological distribution of DMS. The data were generally collected during each hemispheric summer, the BLANES 2022 dataset being the only dataset with close to year-round sampling.

After having examined several alternative model equations and sets of predictors, we adopted a model that used two different linear equations, coined the high and low MeSH:DMS regimes, to predict MeSH from DMS depending on bathymetry and SST cutoff criteria. Compared to more complex multivariate models with nonlinear equations, this simple model based on the separation of high and low MeSH:DMS regimes achieved very similar predictive skill using fewer and more significant model coefficients.

To assess the robustness of the regime cutoff temperature, we randomly subsampled 80% of the observations and varied the temperature cutoff in increments of 1°C between 6° and 15°C. A total of 100 runs with randomly subsampled data was carried out at each temperature cutoff. The slopes and intercepts of the linear regression of model predicted versus the "unseen" 20% of the observations are used to evaluate the temperature cutoff value (fig. S6). Varying the regime cutoff SST revealed that the temperature threshold of 8°C gives the best performance statistics, defined by the predictions versus observations slope (intercept) closest to 1 (0). However, it is nondistinguishable whether a threshold of 8 to 12°C is used. Outside this range, the model performance statistics degrade. Mean ensemble statistics (±95% confidence interval) of the MeSH model runs using cutoff temperatures between 8° and 12°C ($n = 500$) are as follows: high MeSH:DMS regime, slope = 0.294 (0.002), intercept = 0.273 (0.002), and $R^2 = 0.762$ (0.003); low MeSH:DMS regime, slope = 0.094 (0.001), intercept = 0.242 (0.003), and $R^2 = 0.272$ (0.005).

CAM-Chem model experimental setup

The atmospheric component of the Community Earth System Model (CESM) version 1.1.1 (*55*), the Community Atmosphere Model with interactive chemistry (CAM-Chem, version 4) (*34*), was used in this work to evaluate the global impact of oceanic MeSH emission. The CAM-Chem model was used with a spatial resolution of 1.9° in latitude, 2.5° in longitude, and 26 vertical levels from the surface to 3.5 hPa (*34*, *56*). We conducted two different simulations: one that included the global field of MeSH emission flux calculated in the first part of this work, referred to as "MeSH," and a second baseline simulation omitting MeSH emission, referred to as "noMeSH." Both simulations included the same DMS emission inventory.

The "standard" chemical scheme of the CAM-Chem model includes 169 species with comprehensive photochemistry (gas-phase and heterogeneous reactions) and is coupled to the radiation scheme (*55*), which is updated with chemical processing of short-lived halogens. The later includes chlorine, bromine, and iodine species and implements state-of-the-art chemical mechanisms for halogens in the troposphere and stratosphere, broadly validated in previous works (*33*, *57*). In this work, the atmospheric sulfur chemistry scheme was extended to update and include the chemical processing of MeSH. The DMS oxidation scheme in CAM-Chem was updated to include the hydroperoxymethyl thioformate (HPMTF) ($HOOCH_2SCHO$) chemistry [see table S1 in (*51*)]. In addition, the MeSH chemical scheme was implemented following recent works (*26*, *58*) by including the main reactions leading to SO_2 formation (table S1).

Model uncertainties

A set of experiments was also conducted to evaluate the sensitivity of the CAM-Chem model results to the MeSH chemical scheme implemented in the model. The amplifying chemical effect of MeSH on the global VMS burden (34%) was evaluated by varying the chemical kinetics of the dominant MeSH oxidation reaction. Documented upper and lower limit reaction rate values of the dominant MeSH oxidation reaction with OH were considered (*59*), resulting in a ±2.0% confidence range in our result associated with the chemical scheme uncertainty. The uncertainty of the MeSH emission inventory was also assessed. Two sensitivity experiments including the MeSH flux field ± twice the SD obtained from the ensemble-based approach were performed, resulting in a ±4.0% confidence range in our result. Such low uncertainty values underscore the relevant role of MeSH in modulating the atmospheric sulfur cycle and amplifying the aerosol radiative cooling effect reported in this work. On the other hand, the interannual variability of climate conditions, which determine the chemical transport and reaction kinetics, was found to introduce the largest uncertainty in our result (±7.4%). Therefore, to comprehensively represent the reliability of our conclusions, the uncertainty of the CAM-Chem results is expressed in this work as the 95% confidence interval of the annual mean values.

Supplementary Materials

This PDF file includes:

Supplementary Methods
Figs. S1 to S8
Table S1
References

REFERENCES AND NOTES

1. M. A. Moran, B. P. Durham, Sulfur metabolites in the pelagic ocean. *Nat. Rev. Microbiol.* **17**, 665–678 (2019).
2. F. E. Hopkins, S. D. Archer, T. G. Bell, P. Suntharalingam, J. D. Todd, The biogeochemistry of marine dimethylsulfide. *Nat. Rev. Earth Environ.* **4**, 361–376 (2023).
3. P. A. Matrai, M. D. Keller, Total organic sulfur and dimethylsulfoniopropionate in marine phytoplankton: Intracellular variations. *Mar. Biol.* **119**, 61–68 (1994).
4. M. Galí, E. Devred, M. Levasseur, S.-J. Royer, M. Babin, A remote sensing algorithm for planktonic dimethylsulfoniopropionate (DMSP) and an analysis of global patterns. *Remote Sens. Environ.* **171**, 171–184 (2015).
5. R. Simó, Production of atmospheric sulfur by oceanic plankton: Biogeochemical, ecological and evolutionary links. *Trends Ecol. Evol.* **6**, 287–294 (2001).
6. R. P. Kiene, Production of methanethiol from dimethylsulfoniopropionate in marine surface waters. *Mar. Chem.* **54**, 69–83 (1996).
7. R. J. Charlson, J. E. Lovelock, M. O. Andreae, S. G. Warren, Oceanic phytoplankton, atmospheric sulphur, cloud albedo and climate. *Nature* **326**, 655–661 (1987).
8. A. L. Hodshire, P. Campuzano-Jost, J. K. Kodros, B. Croft, B. A. Nault, J. C. Schroder, J. L. Jimenez, J. R. Pierce, The potential role of methanesulfonic acid (MSA) in aerosol formation and growth and the associated radiative forcings. *Atmos. Chem. Phys.* **19**, 3137–3160 (2019).
9. M. O. Andreae, P. J. Crutzen, Atmospheric aerosols: Biogeochemical sources and role in atmospheric chemistry. *Science* **276**, 1052–1058 (1997).
10. M. D. Mallet, R. S. Humphries, S. L. Fiddes, S. P. Alexander, K. Altieri, H. Angot, N. Anilkumar, T. Bartels-Rausch, J. Creamean, M. Dall'Osto, A. Dommergue, M. Frey, S. Henning, D. Lannuzel, R. Lapere, G. G. Mace, A. S. Mahajan, G. M. McFarquhar, K. M. Meiners, B. Miljevic, I. Peeken, A. Protat, J. Schmale, N. Steiner, K. Sellegri, R. Simó, J. L. Thomas, M. D. Willis, V. H. L. Winton, M. T. Woodhouse, Untangling the influence of Antarctic and Southern Ocean life on clouds. *Elem. Sci. Anth.* **11**, 00130 (2023).
11. D. T. McCoy, S. M. Burrows, R. Wood, D. P. Grosvenor, S. M. Elliott, P.-L. Ma, P. J. Rasch, D. L. Hartmann, Natural aerosols explain seasonal and spatial patterns of Southern Ocean cloud albedo. *Sci. Adv.* **1**, e1500157 (2015).
12. K. M. Fung, C. L. Heald, J. H. Kroll, S. Wang, D. S. Jo, A. Gettelman, Z. Lu, X. Liu, R. A. Zaveri, E. C. Apel, D. R. Blake, J.-L. Jimenez, P. Campuzano-Jost, P. R. Veres, T. S. Bates, J. E. Shilling, M. Zawadowicz, Exploring dimethyl sulfide (DMS) oxidation and implications for global aerosol radiative forcing. *Atmos. Chem. Phys.* **22**, 1549–1573 (2022).
13. W. Aas, A. Mortier, V. Bowersox, R. Cherian, G. Faluvegi, H. Fagerli, J. Hand, Z. Klimont, C. Galy-Lacaux, C. M. B. Lehmann, C. L. Myhre, G. Myhre, D. Olivié, K. Sato, J. Quaas, P. S. P. Rao, M. Schulz, D. Shindell, R. B. Skeie, A. Stein, T. Takemura, S. Tsyro, R. Vet, X. Xu, Global and regional trends of atmospheric sulfur. *Sci. Rep.* **9**, 953 (2019).
14. S. Hulswar, R. Simó, M. Galí, T. G. Bell, A. Lana, S. Inamdar, P. R. Halloran, G. Manville, A. S. Mahajan, Third revision of the global surface seawater dimethyl sulfide climatology (DMS-Rev3). *Earth Syst. Sci. Data* **14**, 2963–2987 (2022).

15. R. P. Kiene, L. J. Linn, The fate of dissolved dimethylsulfoniopropionate (DMSP) in seawater: Tracer studies using ^{35}S-DMSP. *Geochim. Cosmochim. Acta* **64**, 2797–2810 (2000).
16. M. Galí, R. Simó, A meta-analysis of oceanic DMS and DMSP cycling processes: Disentangling the summer paradox. *Global Biogeochem. Cycles* **29**, 496–515 (2015).
17. C. R. Reisch, M. J. Stoudemayer, V. A. Varaljay, I. J. Amster, M. A. Moran, W. B. Whitman, Novel pathway for assimilation of dimethylsulphoniopropionate widespread in marine bacteria. *Nature* **473**, 208–211 (2011).
18. M. Landa, A. S. Burns, B. P. Durham, K. Esson, B. Nowinski, S. Sharma, A. Vorobev, T. Nielsen, R. P. Kiene, M. A. Moran, Sulfur metabolites that facilitate oceanic phytoplankton–bacteria carbon flux. *ISME J.* **13**, 2536–2550 (2019).
19. J. Sun, J. D. Todd, J. C. Thrash, Y. Qian, M. C. Qian, B. Temperton, J. Guo, E. K. Fowler, J. T. Aldrich, C. D. Nicora, M. S. Lipton, R. D. Smith, P. De Leenheer, S. H. Payne, A. W. B. Johnston, C. L. Davie-Martin, K. H. Halsey, S. J. Giovannoni, The abundant marine bacterium Pelagibacter simultaneously catabolizes dimethylsulfoniopropionate to the gases dimethyl sulfide and methanethiol. *Nat. Microbiol.* **1**, 16065 (2016).
20. H. Schäfer, Ö. Eyice, Microbial cycling of methanethiol. *Curr. Issues Mol. Biol.* **33**, 173–182 (2019).
21. H. Bürgmann, E. C. Howard, W. Ye, F. Sun, S. Sun, S. Napierala, M. A. Moran, Transcriptional response of Silicibacter pomeroyi DSS-3 to dimethylsulfoniopropionate (DMSP). *Environ. Microbiol.* **9**, 2742–2755 (2007).
22. X.-Y. He, N.-H. Liu, J.-Q. Liu, M. Peng, Z.-J. Teng, T.-J. Gu, X.-L. Chen, Y. Chen, P. Wang, C.-Y. Li, J. D. Todd, Y.-Z. Zhang, X.-Y. Zhang, SAR92 clade bacteria are potentially important DMSP degraders and sources of climate-active gases in marine environments. *mBio* **14**, e01467-23 (2023).
23. A. J. Kettle, T. S. Rhee, M. von Hobe, A. Poulton, J. Aiken, M. O. Andreae, Assessing the flux of different volatile sulfur gases from the ocean to the atmosphere. *J. Geophys. Res. Atmos.* **106**, 12193–12209 (2001).
24. V. Gros, B. Bonsang, R. Sarda-Estève, A. Nikolopoulos, K. Metfies, M. Wietz, I. Peeken, Concentrations of dissolved dimethyl sulfide (DMS), methanethiol and other trace gases in context of microbial communities from the temperate Atlantic to the Arctic Ocean. *Biogeosciences* **20**, 851–867 (2023).
25. S. J. Lawson, C. S. Law, M. J. Harvey, T. G. Bell, C. F. Walker, W. J. de Bruyn, E. S. Saltzman, Methanethiol, dimethyl sulfide and acetone over biologically productive waters in the southwest Pacific Ocean. *Atmos. Chem. Phys.* **20**, 3061–3078 (2020).
26. G. A. Novak, D. B. Kilgour, C. M. Jernigan, M. P. Vermeuel, T. H. Bertram, Oceanic emissions of dimethyl sulfide and methanethiol and their contribution to sulfur dioxide production in the marine atmosphere. *Atmos. Chem. Phys.* **22**, 6309–6325 (2022).
27. D. B. Kilgour, C. M. Jernigan, S. Zhou, E. Brito de Azevedo, J. Wang, M. A. Zawadowicz, T. H. Bertram, Contribution of speciated monoterpenes to secondary aerosol in the Eastern North Atlantic. *ACS EST Air* **1**, 789–800 (2024).
28. D. B. Kilgour, G. A. Novak, J. S. Sauer, A. N. Moore, J. Dinasquet, S. Amiri, E. B. Franklin, K. Mayer, M. Winter, C. K. Morris, T. Price, F. Malfatti, D. R. Crocker, C. Lee, C. D. Cappa, A. H. Goldstein, K. A. Prather, T. H. Bertram, Marine gas-phase sulfur emissions during an induced phytoplankton bloom. *Atmos. Chem. Phys.* **22**, 1601–1613 (2022).
29. Intergovernmental Panel On Climate Change, *Climate Change 2021–The Physical Science Basis: Working Group I Contribution to the Sixth Assessment Report of the Intergovernmental Panel on Climate Change* (Cambridge Univ. Press, ed. 1, 2023).
30. C. Wohl, Q. Güell-Bujons, Y. M. Castillo, A. Calbet, R. Simó, Volatile organic compounds released by *Oxyrrhis marina* grazing on *Isochrysis galbana*. *Oceans* **4**, 151–169 (2023).
31. O. R. Flöck, M. O. Andreae, Photochemical and non-photochemical formation and destruction of carbonyl sulfide and methyl mercaptan in ocean waters. *Mar. Chem.* **54**, 11–26 (1996).
32. V. S. Ulshöfer, O. R. Flock, G. Uher, M. O. Andreae, Photochemical production and air-sea exchange of carbonyl sulfide in the eastern Mediterranean Sea. *Mar. Chem.* **53**, 25–39 (1996).
33. A. Saiz-Lopez, R. P. Fernandez, Q. Li, C. A. Cuevas, X. Fu, D. E. Kinnison, S. Tilmes, A. S. Mahajan, J. C. Gómez Martín, F. Iglesias-Suarez, R. Hossaini, J. M. C. Plane, G. Myhre, J.-F. Lamarque, Natural short-lived halogens exert an indirect cooling effect on climate. *Nature* **618**, 967–973 (2023).
34. J.-F. Lamarque, L. K. Emmons, P. G. Hess, D. E. Kinnison, S. Tilmes, F. Vitt, C. L. Heald, E. A. Holland, P. H. Lauritzen, J. Neu, J. J. Orlando, P. J. Rasch, G. K. Tyndall, CAM-chem: Description and evaluation of interactive atmospheric chemistry in the Community Earth System Model. *Geosci. Model Dev.* **5**, 369–411 (2012).
35. G. Myhre, W. Aas, R. Cherian, W. Collins, G. Faluvegi, M. Flanner, P. Forster, Ø. Hodnebrog, Z. Klimont, M. T. Lund, J. Mülmenstädt, C. L. Myhre, D. Olivié, M. Prather, J. Quaas, B. H. Samset, J. L. Schnell, M. Schulz, D. Shindell, R. B. Skeie, T. Takemura, S. Tsyro, Multi-model simulations of aerosol and ozone radiative forcing due to anthropogenic emission changes during the period 1990–2015. *Atmos. Chem. Phys.* **17**, 2709–2720 (2017).
36. Y. Yang, H. Wang, S. J. Smith, R. Easter, P.-L. Ma, Y. Qian, H. Yu, C. Li, P. J. Rasch, Global source attribution of sulfate concentration and direct and indirect radiative forcing. *Atmos. Chem. Phys.* **17**, 8903–8922 (2017).
37. A. Rap, C. E. Scott, D. V. Spracklen, N. Bellouin, P. M. Forster, K. S. Carslaw, A. Schmidt, G. Mann, Natural aerosol direct and indirect radiative effects. *Geophys. Res. Lett.* **40**, 3297–3301 (2013).
38. A. Bodas-Salcedo, K. D. Williams, M. A. Ringer, I. Beau, J. N. S. Cole, J.-L. Dufresne, T. Koshiro, B. Stevens, Z. Wang, T. Yokohata, Origins of the solar radiation biases over the Southern Ocean in CFMIP2 models. *J. Clim.* **27**, 41–56 (2014).
39. S. L. Fiddes, A. Protat, M. D. Mallet, S. P. Alexander, M. T. Woodhouse, Southern Ocean cloud and shortwave radiation biases in a nudged climate model simulation: Does the model ever get it right? *Atmos. Chem. Phys.* **22**, 14603–14630 (2022).
40. A. J. Schuddeboom, A. J. McDonald, The Southern Ocean radiative bias, cloud compensating errors, and equilibrium climate sensitivity in CMIP6 models. *J. Geophys. Res. Atmos.* **126**, e2021JD035310 (2021).
41. Q. Li, R. P. Fernandez, R. Hossaini, F. Iglesias-Suarez, C. A. Cuevas, E. C. Apel, D. E. Kinnison, J.-F. Lamarque, A. Saiz-Lopez, Reactive halogens increase the global methane lifetime and radiative forcing in the 21st century. *Nat. Commun.* **13**, 2768 (2022).
42. C. Wohl, Q. Li, C. A. Cuevas, R. P. Fernandez, M. Yang, A. Saiz-Lopez, R. Simó, Marine biogenic emissions of benzene and toluene and their contribution to secondary organic aerosols over the polar oceans. *Sci. Adv.* **9**, eadd9031 (2023).
43. V. Ferracci, J. Weber, C. G. Bolas, A. D. Robinson, F. Tummon, P. Rodríguez-Ros, P. Cortés-Greus, A. Baccarini, R. L. Jones, M. Galí, R. Simó, J. Schmale, N. R. P. Harris, Atmospheric isoprene measurements reveal larger-than-expected Southern Ocean emissions. *Nat. Commun.* **15**, 2571 (2024).
44. L. Bopp, O. Boucher, O. Aumont, S. Belviso, J.-L. Dufresne, M. Pham, P. Monfray, Will marine dimethylsulfide emissions amplify or alleviate global warming? A model study. *Can. J. Fish. Aquat. Sci.* **61**, 826–835 (2004).
45. A. Gabric, B. Qu, L. Rotstayn, J. Shephard, Global simulations of the impact on contemporary climate of a perturbation to the sea-to-air flux of dimethylsulfide. *Aust. Meteorol. Oceanogr. J.* **63**, 365–376 (2013).
46. S. Wang, M. E. Maltrud, S. M. Burrows, S. M. Elliott, P. Cameron-Smith, Impacts of shifts in phytoplankton community on clouds and climate via the sulfur cycle. *Global Biogeochem. Cycles* **32**, 1005–1026 (2018).
47. S. M. Vallina, R. Simó, Strong relationship between DMS and the solar radiation dose over the global surface ocean. *Science* **315**, 506–508 (2007).
48. A. Lana, R. Simó, S. M. Vallina, J. Dachs, Potential for a biogenic influence on cloud microphysics over the ocean: A correlation study with satellite-derived data. *Atmos. Chem. Phys.* **12**, 7977–7993 (2012).
49. P. K. Quinn, T. S. Bates, The case against climate regulation via oceanic phytoplankton sulphur emissions. *Nature* **480**, 51–56 (2011).
50. P. K. Quinn, D. J. Coffman, J. E. Johnson, L. M. Upchurch, T. S. Bates, Small fraction of marine cloud condensation nuclei made up of sea spray aerosol. *Nat. Geosci.* **10**, 674–679 (2017).
51. P. R. Veres, J. A. Neuman, T. H. Bertram, E. Assaf, G. M. Wolfe, C. J. Williamson, B. Weinzierl, S. Tilmes, C. R. Thompson, A. B. Thames, J. C. Schroder, A. Saiz-Lopez, A. W. Rollins, J. M. Roberts, D. Price, J. Peischl, B. A. Nault, K. H. Møller, D. O. Miller, S. Meinardi, Q. Li, J.-F. Lamarque, A. Kupc, H. G. Kjaergaard, D. Kinnison, J. L. Jimenez, C. M. Jernigan, R. S. Hornbrook, A. Hills, M. Dollner, D. A. Day, C. A. Cuevas, P. Campuzano-Jost, J. Burkholder, T. P. Bui, W. H. Brune, S. S. Brown, C. A. Brock, I. Bourgeois, D. R. Blake, E. C. Apel, T. B. Ryerson, Global airborne sampling reveals a previously unobserved dimethyl sulfide oxidation mechanism in the marine atmosphere. *Proc. Natl. Acad. Sci. U.S.A.* **117**, 4505–4510 (2020).
52. K. Goto-Azuma, M. Hirabayashi, H. Motoyama, T. Miyake, T. Kuramoto, R. Uemura, M. Igarashi, Y. Iizuka, T. Sakurai, S. Horikawa, K. Suzuki, T. Suzuki, K. Fujita, Y. Kondo, S. Hattori, Y. Fujii, Reduced marine phytoplankton sulphur emissions in the Southern Ocean during the past seven glacials. *Nat. Commun.* **10**, 3247 (2019).
53. C. Wohl, D. Capelle, A. Jones, W. T. Sturges, P. D. Nightingale, B. G. T. Else, M. Yang, Segmented flow coil equilibrator coupled to a proton-transfer-reaction mass spectrometer for measurements of a broad range of volatile organic compounds in seawater. *Ocean Sci.* **15**, 925–940 (2019).
54. J. B. Burkholder, S. P. Sander, J. P. D. Abbatt, J. R. Barker, C. D. Cappa, J. D. Crounse, T. S. Dibble, R. E. Huie, C. E. Kolb, M. J. Kurylo, V. L. Orkin, C. J. Percival, D. M. Wilmouth, P. H. Wine, Chemical Kinetics and Photochemical Data for Use in Atmospheric Studies, Evaluation No. 19 (JPL Publication, 2019); http://jpldataeval.jpl.nasa.gov.
55. S. Tilmes, J.-F. Lamarque, L. K. Emmons, D. E. Kinnison, D. Marsh, R. R. Garcia, A. K. Smith, R. R. Neely, A. Conley, F. Vitt, M. Val Martin, H. Tanimoto, I. Simpson, D. R. Blake, N. Blake, Representation of the Community Earth System Model (CESM1) CAM4-chem within the Chemistry-Climate Model Initiative (CCMI). *Geosci. Model Dev.* **9**, 1853–1890 (2016).
56. R. B. Neale, J. Richter, S. Park, P. H. Lauritzen, S. J. Vavrus, P. J. Rasch, M. Zhang, The mean climate of the Community Atmosphere Model (CAM4) in forced SST and fully coupled experiments. *J. Clim.* **26**, 5150–5168 (2013).
57. R. P. Fernandez, A. Carmona-Balea, C. A. Cuevas, J. A. Barrera, D. E. Kinnison, J.-F. Lamarque, C. Blaszczak-Boxe, K. Kim, W. Choi, T. Hay, A.-M. Blechschmidt, A. Schönhardt, J. P. Burrows, A. Saiz-Lopez, Modeling the sources and chemistry of polar

tropospheric halogens (Cl, Br, and I) using the CAM-Chem global chemistry-climate model. *J. Adv. Model. Earth Syst.* **11**, 2259–2289 (2019).
58. T. Berndt, E. H. Hoffmann, A. Tilgner, F. Stratmann, H. Herrmann, Direct sulfuric acid formation from the gas-phase oxidation of reduced-sulfur compounds. *Nat. Commun.* **14**, 4849 (2023).
59. R. Atkinson, D. L. Baulch, R. A. Cox, J. N. Crowley, R. F. Hampson, R. G. Hynes, M. E. Jenkin, M. J. Rossi, J. Troe, Evaluated kinetic and photochemical data for atmospheric chemistry: Volume I - gas phase reactions of O_x, HO_x, NO_x and SO_x species. *Atmos. Chem. Phys.* **4**, 1461–1738 (2004).
60. M. T. Johnson, A numerical scheme to calculate temperature and salinity dependent air-water transfer velocities for any gas. *Ocean Sci.* **6**, 913–932 (2010).
61. F. Gharagheizi, Determination of diffusion coefficient of organic compounds in water using a simple molecular-based method. *Ind. Eng. Chem. Res.* **51**, 2797–2803 (2012).
62. M. Yang, B. W. Blomquist, C. W. Fairall, S. D. Archer, B. J. Huebert, Air-sea exchange of dimethylsulfide in the Southern Ocean: Measurements from SO GasEx compared to temperate and tropical regions. *J. Geophys. Res. Oceans* **116**, 2010JC006526 (2011).
63. M. Yang, P. D. Nightingale, R. Beale, P. S. Liss, B. Blomquist, C. Fairall, Atmospheric deposition of methanol over the Atlantic Ocean. *Proc. Natl. Acad. Sci. U.S.A.* **110**, 20034–20039 (2013).
64. C.-L. Lee, P. Brimblecombe, Anthropogenic contributions to global carbonyl sulfide, carbon disulfide and organosulfides fluxes. *Earth Sci. Rev.* **160**, 1–18 (2016).
65. J. W. Hurrell, J. J. Hack, D. Shea, J. M. Caron, J. Rosinski, A new sea surface temperature and sea ice boundary dataset for the Community Atmosphere Model. *J. Clim.* **21**, 5145–5153 (2008).
66. W.-L. Wang, G. Song, F. Primeau, E. S. Saltzman, T. G. Bell, J. K. Moore, Global ocean dimethyl sulfide climatology estimated from observations and an artificial neural network. *Biogeosciences* **17**, 5335–5354 (2020).
67. D. Joge, A. S. Mahajan, S. Hulswar, C. A. Marandino, M. Galí, T. G. Bell, M. Yang, R. Simó, Dimethyl sulfide (DMS) climatologies, fluxes, and trends—Part 2: Sea-air fluxes. *Biogeosciences* **21**, 4453–4467 (2024).
68. A. Lana, T. G. Bell, R. Simó, S. M. Vallina, J. Ballabrera-Poy, A. J. Kettle, J. Dachs, L. Bopp, E. S. Saltzman, J. Stefels, J. E. Johnson, P. S. Liss, An updated climatology of surface dimethlysulfide concentrations and emission fluxes in the global ocean. *Global Biogeochem. Cycles* **25**, 2010GB003850 (2011).
69. J.-E. Tesdal, J. R. Christian, A. H. Monahan, K. von Salzen, Evaluation of diverse approaches for estimating sea-surface DMS concentration and air–sea exchange at global scale. *Environ. Chem.* **13**, 390–412 (2015).
70. T. G. Bell, S. Landwehr, S. D. Miller, W. J. de Bruyn, A. H. Callaghan, B. Scanlon, B. Ward, M. Yang, E. S. Saltzman, Estimation of bubble-mediated air-sea gas exchange from concurrent DMS and CO_2 transfer velocities at intermediate-high wind speeds. *Atmos. Chem. Phys.* **17**, 9019–9033 (2017).
71. S. J. Ghan, Technical Note: Estimating aerosol effects on cloud radiative forcing. *Atmos. Chem. Phys.* **13**, 9971–9974 (2013).
72. A. A. Lacis, J. E. Hansen, G. L. Russell, V. Oinas, J. Jonas, The role of long-lived greenhouse gases as principal LW control knob that governs the global surface temperature for past and future climate change. *Tellus B Chem. Phys. Meteorol.* **65**, 19734 (2013).
73. M. J. Iacono, J. S. Delamere, E. J. Mlawer, M. W. Shephard, S. A. Clough, W. D. Collins, Radiative forcing by long-lived greenhouse gases: Calculations with the AER radiative transfer models. *J. Geophys. Res. Atmos.* **113**, 2008JD009944 (2008).

Acknowledgments: To the memory of Ron Kiene, in gratitude for his pioneering, thorough, and inspirational work on marine MeSH. We especially thank I. Peeken (AWI, chief scientist on TRANSSIZ), B. Bonsang (LSCE), C. Cardelús (ICM-CSIC, operating the BBMO), and M. Dall'Osto (ICM-CSIC, chief scientist on POLAR-CHANGE). This work represents a contribution to the CSIC Interdisciplinary Thematic Platform (PTI) Polar zone Observatory (POLAR-CSIC). **Funding:** This work was supported by the European Research Council Executive Agency ERC-2018-AdG 834162 SUMMIT (R.S.), European Research Council Executive Agency ERC-2016-COG 726349 CLIMAHAL (A.S.-L.), Spanish Ministry of Science and Innovation (MCIN/AEI/10.13039/501100011033) grant PID2022-140872NB-I00 GOOSE (R.S. and M.G.), Spanish Ministry of Science and Innovation "Severo Ochoa Centre of Excellence" CEX2019-000928-S (ICM), CONICET and ANPCyT Argentina grants PICT 2019-2187 and PICT 2022-0474 (R.P.F.), National Science Foundation (United States) via the CESM project, Alfred Wegener Institute (AWI) for the TRANSSIZ expedition ARK XXIX/1 grant AWI_PS92_00 (V.G. and R.S.-E.), NRBC-E Research & Development programme France via the BioChemicalCollectors (BCC) project (V.G. and R.S.-E.), CNRS-INSU (V.G. and R.S.-E.), and Ministry of Earth Sciences, Government of India (A.S.M.). **Author contributions:** Conceptualization: R.S. and A.S.-L. Data curation: M.G., C.W., and J.V. Methodology: M.G., C.W., R.S., J.V., R.P.F., C.A.C., A.B., Q.L., and A.S.-L. Investigation: C.W., M.G., J.V., A.J.K., T.W., R.S.-E., V.G., R.P.F., R.S., and A.S.-L. Funding acquisition: A.S.-L., R.S., and M.G. Writing—original draft: C.W., J.V., M.G., R.S., and A.S.-L. Writing—review and editing: A.S.M., R.P.F., C.A.C., A.B., Q.L., A.J.K., T.W., R.S.-E., and V.G. **Competing interests:** The authors declare that they have no competing interests. **Data and materials availability:** All data needed to evaluate the conclusions in the paper are present in the paper and/or the Supplementary Materials. POLAR-CHANGE 2023 (https://doi.org/10.5281/zenodo.12758980), Blanes 2022 (https://doi.org/10.5281/zenodo.12758703), and AMT-7 (https://doi.org/10.5281/zenodo.12759178) can be downloaded online. Monthly maps of concentrations and sea-to-air fluxes of MeSH are available in Zenodo (https://doi.org/10.5281/zenodo.12943019). The public version of the CAM-Chem software used in this work is available for download from https://www2.acom.ucar.edu/gcm/cam-chem. The CAM-Chem output data related to this article are available in Mendeley (https://data.mendeley.com/datasets/7wy65833v5/1).

Submitted 4 May 2024
Accepted 24 October 2024
Published 27 November 2024
10.1126/sciadv.adq2465